



Biomass-Based Polymer Nanoparticles With Aggregation-Induced Fluorescence Emission for Cell Imaging and Detection of Fe³⁺ Ions

Shiyan Han^{1,2}, Jiixin Ni^{2†}, Youqi Han^{2†}, Min Ge², Chunlei Zhang², Guiquan Jiang³, Zhibin Peng⁴, Jun Cao^{1*} and Shujun Li^{2*}

¹ Postdoctoral Station of Mechanical Engineering, Northeast Forestry University, Harbin, China, ² Key Laboratory of Bio-Based Material Science and Technology (Northeast Forestry University), Ministry of Education, Harbin, China, ³ Key Laboratory of Wooden Materials Science and Engineering of Jilin Province, Beihua University, Jilin, China, ⁴ Department of Orthopedic Surgery, The First Affiliated Hospital of Harbin Medical University, Harbin, China

OPEN ACCESS

Edited by:

Alfonso Jiménez,
University of Alicante, Spain

Reviewed by:

Artur J. M. Valente,
University of Coimbra, Portugal
Lei Yang,
Arkema, United States

*Correspondence:

Jun Cao
zdhcj@126.com
Shujun Li
lishujun@nefu.edu.cn

[†]These authors have contributed
equally to this work

Specialty section:

This article was submitted to
Polymer Chemistry,
a section of the journal
Frontiers in Chemistry

Received: 13 March 2020

Accepted: 02 June 2020

Published: 03 July 2020

Citation:

Han S, Ni J, Han Y, Ge M, Zhang C,
Jiang G, Peng Z, Cao J and Li S
(2020) Biomass-Based Polymer
Nanoparticles With
Aggregation-Induced Fluorescence
Emission for Cell Imaging and
Detection of Fe³⁺ Ions.
Front. Chem. 8:563.
doi: 10.3389/fchem.2020.00563

Polymeric nanoparticles, which show aggregation-induced luminescence emission, have been successfully prepared from larch bark, a natural renewable biomass resource, in a simple, rapid ultrasonic fragmentation method. The structure, element, particle size and molecular weight distribution of larch bark extracts (LBE) were studied by FTIR, XPS, TEM, XRD and linear mode mass spectrometry, respectively. LBE was found containing large numbers of aromatic rings, displaying an average particle size of about 4.5 nm and mainly presenting tetramers proanthocyanidins. High concentration, poor solvent, low temperature and high viscosity restricted the rotation and vibration of the aromatic rings in LBE, leading to the formation of J-aggregates and enhancing the aggregation-induced fluorescence emission. LBE possessed good resistance to photobleaching under ultraviolet light (200 mW/m²). Cytotoxicity experiments for 24 h and flow cytometry experiments for 3 days proved that even the concentrations of LBE as high as 1 mg/mL displayed non-toxic to MG-63 cells. Therefore, LBE could be employed for MG-63 cell imaging, with similar nuclear staining to the DAPI. The effects of different metal ions on the fluorescence emission intensity of LBE were analyzed and exhibited that Fe³⁺ owned obvious fluorescence quenching effect on LBE, while other metal ions possessed little or weak effect. Furthermore, the limit of detection (LOD) of Fe³⁺ was evaluated as 0.17 μM.

Keywords: larch bark, polymeric nanoparticles, aggregation-induced emission, cellular imaging, fluorescent probe for Fe³⁺

INTRODUCTION

Fluorescent nanoparticles, including organic molecules (Lou et al., 2016; Zhang et al., 2017) graphene quantum dots (Zhu et al., 2016) and carbon dots (Wang et al., 2014; Chang et al., 2019), possess low toxicity and good biocompatibility, and are resistant to photobleaching, which exhibit enormous potential in cellular and *in vivo* imaging (Wang et al., 2013; Ding et al., 2016, 2018; He et al., 2018), as fluorescent probes (Qu et al., 2013; Zhang et al., 2014; Li et al., 2019a; Qi et al., 2019), in light-emitting diodes (Chiung et al., 2005; Lee et al., 2016; Tachibana et al., 2017; Liu et al., 2018; Wu et al., 2019), as ultraviolet and blue light blockers (Park et al., 2019)

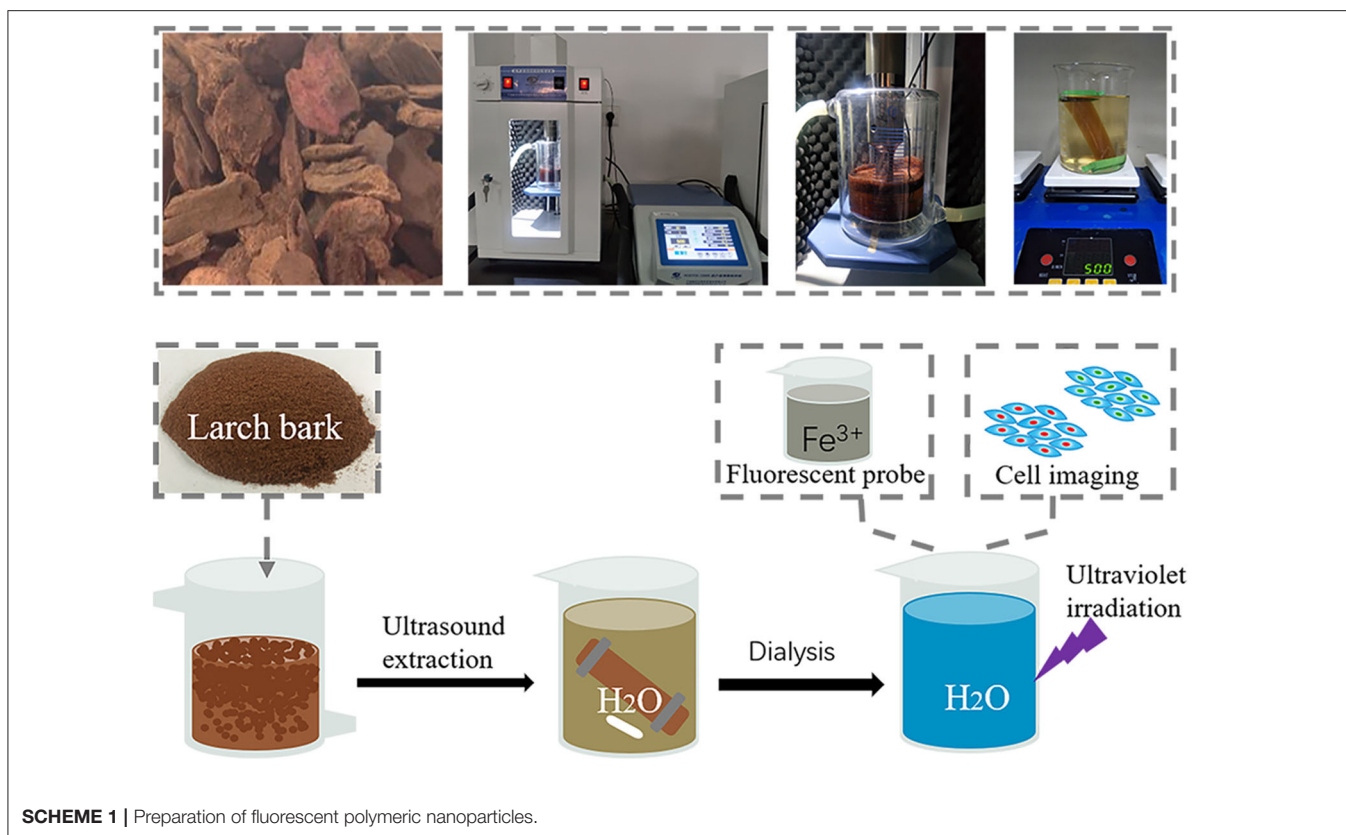
and for the detection of counterfeit materials (Chen et al., 2017). At present, organic molecules fluorescent nanoparticles are most commonly used in the field of cellular imaging and fluorescent probes. Especially researches into organic molecule-based nanoparticles with aggregation-induced emission (AIE) in cellular imaging have made especially good progress, duo to high selectivity, high sensitivity and good biocompatibility (Hu et al., 2014; He et al., 2018). Better AIE performance can be achieved with polymeric molecules than that with small organic molecules because the structure, morphology and function of the polymers can be fine-tuned, thus can be employed in cellular imaging and as fluorescent probes (Wang et al., 2013; Gu et al., 2016). Although much progress have been made in the study of fluorescent nanoparticles based on organic molecules, many challenges remain still to be accomplished. Most small molecule-based and polymeric fluorescent nanoparticles require expensive and time-consuming synthesis and toxic reagents, which limit their wide applications. The preparation of polymeric nanoparticles with AIE property by simple extraction of renewable natural raw material would be very attractive, which was paid little concern. Biomass resources have been extensively studied because of their excellent properties such as wide sources, non-toxic, renewable and so on (An et al., 2019; Du et al., 2019; Li et al., 2019c), in addition, they are also used as raw materials for the preparation of fluorescent materials due to their own sustainability (He et al., 2018; Li et al., 2019b). Larch bark is typically regarded as waste, but larch bark extracts (LBE) contain large amounts of catechol-containing compounds (Jiang et al., 2014, 2016; Luo et al., 2019). In previous reports, LBE have many medicinal values and are used as a free radical scavengers, antioxidants and anti-tumor drugs (Sharma et al., 2010; Ouchemoukh et al., 2012; Jiang et al., 2014, 2016). The application of LBE fluorescence in the field of metal ion probe and biological imaging has not been reported. In this study, therefore, the green and cheap larch bark was chosen as the raw material to produce polymeric nanoparticles with AIE property. A time saving procedure was designed adopting 40% ethanol as the extraction solvent and ultrasonic crushing as the extraction method. The resulting polymeric nanoparticles owned good biocompatibility and potential both for cellular imaging and for the detection of ferric ions (Fe^{3+} ; Scheme 1). Our method for producing natural polymeric nanoparticles with AIE from the rational use of larch bark, could be regarded as a process turning waste into wealth.

RESULTS AND DISCUSSION

Larch bark extracts (LBE) containing oligomeric proanthocyanidins was extracted from larch bark using the ultrasonic crushing method, with 40% aqueous ethanol as the extraction solvent and (Jiang et al., 2016; Luo et al., 2019), through dialysis (3,500 Dalton) and freeze-drying. The structure of LBE was analyzed by FT-IR spectroscopy, XPS, UV spectroscopy and mass spectrometry. The FT-IR spectrum (Figure 1A) illustrated that LBE contained hydroxyl groups ($3,285\text{ cm}^{-1}$), $-\text{CH}_3/-\text{CH}_2$ groups ($2,934$ and $2,880$

cm^{-1}), benzene rings ($1,608$, $1,510$ and $1,446\text{ cm}^{-1}$), $-\text{CH}_3$ groups ($1,362\text{ cm}^{-1}$), carbonyl groups ($1,784$ and $1,710\text{ cm}^{-1}$), C-O-C bonds ($1,246\text{ cm}^{-1}$) and aromatic hydroxyl groups ($1,064\text{ cm}^{-1}$; Bao et al., 2015; Zhang et al., 2018). XPS analysis showed that LBE contained C (46%) and O (54%) elements (Figure 1B). Following analysis of the high resolution XPS spectra of elemental C (Figure 1C) and O (Figure 1D), the binding energies of 532.28, 286, and 284.5 eV were attributed to O-C, C-O, and C-C/C=C bonds, respectively (Sheng et al., 2011; He et al., 2018; Miao et al., 2018; Zhang et al., 2018). The UV absorption spectrum of LBE (Figure 1E) contained $n-\pi^*$ and $\pi-\pi^*$ transitions between 190 and 400 nm (Bi et al., 2018; Miao et al., 2018). The molecular weight distribution of LBE was analyzed by linear mode MALDI-TOF mass spectrometry after deionization and addition of Cs^{3+} as cationic reagent (Shoji et al., 2006; María et al., 2010; Jara and Josep, 2012). The primordial series of proanthocyanidins ion peaks (Figure 1F) showed a fixed difference of 288a. The difference between the observed value and the calculated value was compared using the equation $m/z = 290 + 288a + 133$ (Yang and Chien, 2000; Krueger et al., 2003), where 290 is the relative molecular mass of the terminal epicatechin unit, 288 is the relative molecular mass of extending epicatechin units, 133 is the relative atomic mass of Cs^+ and a is the degree of polymerization. The analysis demonstrated that LBE is a mixture of oligomers proanthocyanidins (Figure 1E), ranging from trimer (m/z 999.7) to nonamer (m/z 2737.7), with the strongest ion peak for the tetramer (m/z 1287; Figure 1F), indicating that LBE mainly consists of tetramers proanthocyanidins.

Fluorescence analysis of LBE was carried out in water proven to be a good solvent. Measurement of fluorescence emission in an aqueous solution of LBE at different excitation wavelengths showed that the optimal excitation wavelength is 330 nm with an emission peak of 400 nm (Figure S1). Fluorescence emission of LBE exhibited excitation dependence. An aqueous solution of LBE displayed blue fluorescence irradiated with ultraviolet light (365 nm; Figure S2). The fluorescence intensity of LBE increased with the increasing concentration over the range from 0.1 to $10\text{ }\mu\text{g/mL}$ (Figures 2A,B). Ultraviolet absorption also increased and red shift with the increasing concentration (Figure S3). The enhanced fluorescence emission at higher concentrations occurred because the LBE molecules moved closer to each other, restricting rotation and vibration of the large aromatic rings in the molecules and thus resulting in the enhanced aggregation-induced fluorescence emission (Hu et al., 2014; Mei et al., 2014; He et al., 2018). The aggregation induced luminescence of LBE by mixing of good solvent (water) and poor solvent (DMSO and EtOH) was further studied. The results showed that the fluorescence emission intensity of the solution increased as the volume ratio of DMSO increased (Figures 2C,D). In the mixed system of water and DMSO, water clusters and hydrophobic DMSO clusters are formed in the mixed solvent (Zhang N. et al., 2013; Gujt et al., 2017). When the proportion of DMSO is increased, the hydrophilic LBE fluorophore molecules are aggregated in the mixed solvent by the hydrophobic DMSO clusters to form nanoparticles, which limits or restricts the intramolecular

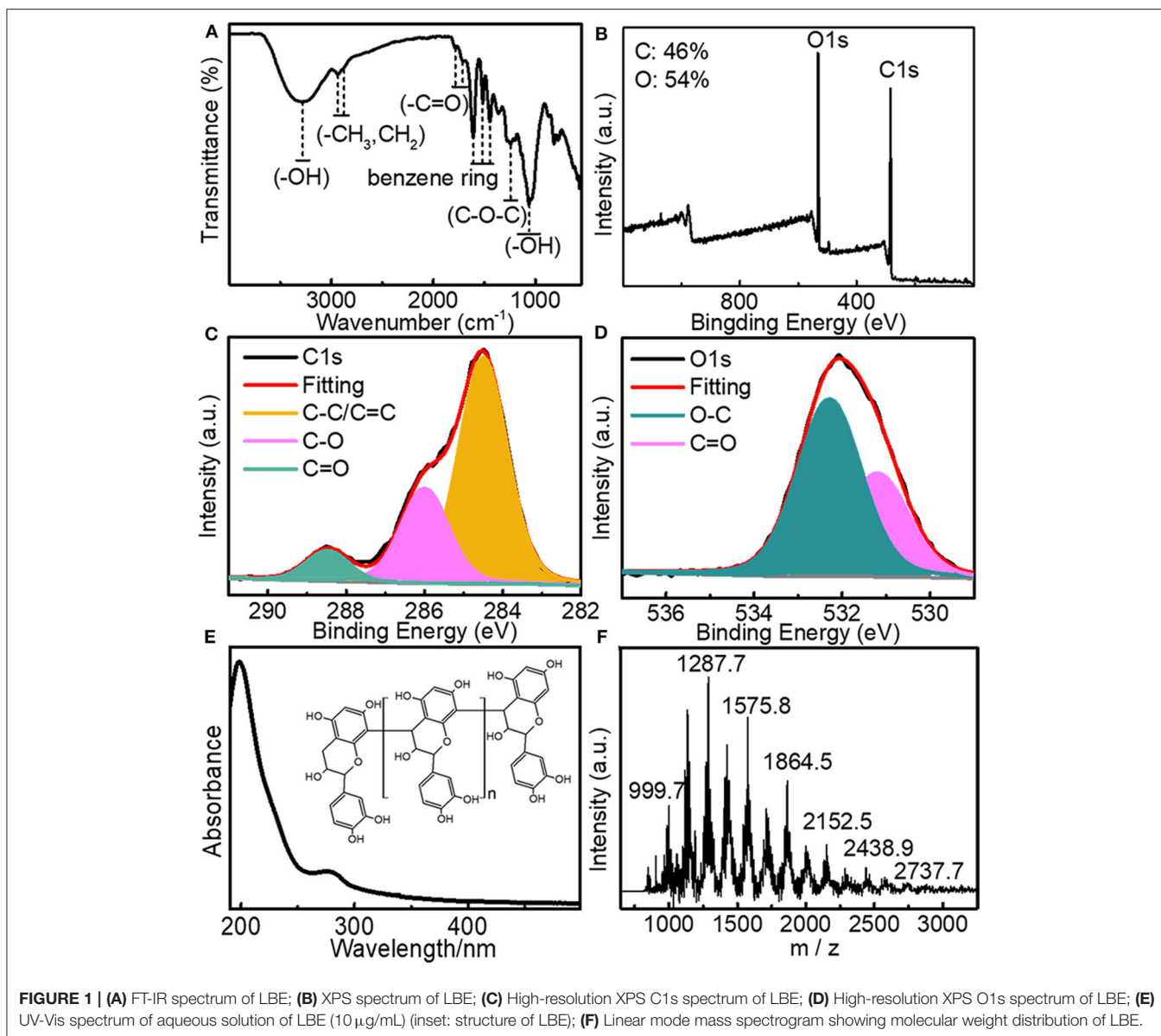


rotation of the LBE fluorophore, leading to the closing of non-radiative attenuation channels and the enhancement of fluorescence emission (Lu et al., 2012; Mei et al., 2014; He et al., 2018; Yang et al., 2019), also, it is the typical feature of the AIE phenomenon (Hong et al., 2009; Lu et al., 2012). Moreover, when the volume ratio of ethanol as poor solvent in the solvent increased, LBE also showed aggregation induced emission (AIE; Figures 2E,F).

The luminescence mechanism was further investigated by high-resolution transmission electron microscopy (HR-TEM) of LBE dispersed in water (Figure 3). The TEM image showed a lattice spacing of 0.21 nm, which corresponded to the [100] facet of graphene-like structures (Chen et al., 2016). The particle size distributed in the range 2–8 nm, with an average diameter of ~4.5 nm (Figures 3A,B). The XRD pattern of LBE (Figure S4) illustrated an apparent peak at $\sim 21.7^\circ$, which was attributed to an interlayer spacing of 0.34 nm, corresponding to the [002] facet of graphene-like structures (Zhu et al., 2013; Bi et al., 2018). The particles exhibited marked aggregation on addition of DMSO (Figure 3C) or ethanol (Figure 3D) to an aqueous solution, resulting in enhanced aggregate luminescence, which possessed luminescence characteristics similar to those of AIE (Hu et al., 2014; He et al., 2018). The photoluminescence quantum yield (PLQY) of LBE in water, DMSO and ethanol were 2.96, 3.25, and 3.72%, respectively.

To further investigate the luminescence properties of LBE, the effect of viscosity and temperature on the fluorescence intensity

of LBE were analyzed. The fluorescence emission intensity of LBE increased with the increase of glycerol content when the water and glycerin were synergistically chosen to adjust solution viscosity with different volume ratios (Figure 4A and Figure S5), which mainly due to the high viscosity of the solvent limiting the rotation of the aromatic rings of LBE molecule, leading to an increment in the radiation transition, thus the LBE molecules show aggregation induced emission enhancement. The fluorescence intensity decreased with increasing temperature from 0 to 60°C (Figure 4B and Figure S6). The changes in fluorescence emission intensity with temperature occurred because the rotation of the macromolecular aromatic rings of LBE was restricted at lower temperatures, preventing non-radiative transitions and increasing fluorescence emission through radiative transitions (He et al., 2018). The resistance of LBE fluorescence to photobleaching was then investigated. The fluorescence intensity of an aqueous solution of LBE was reduced by about 20% after 30 min under strong ultraviolet light (200 mW/m^2) and maintained further after continuous irradiation for 180 min (Figure 4C and Figure S7A). For comparison, the fluorescence intensity of the commercially available fluorescent stain 4',6-diamidino-2-phenylindole (DAPI) was reduced by ~83% after irradiation for 180 min (Figure 4C and Figure S7B). It is worth noting that the intensity of the UV irradiance used here was 200 mW/cm^2 , which is 2,000-fold higher than the intensity used in a recent study (He et al., 2018). The fluorescence intensity of the LBE was stable, over the pH range



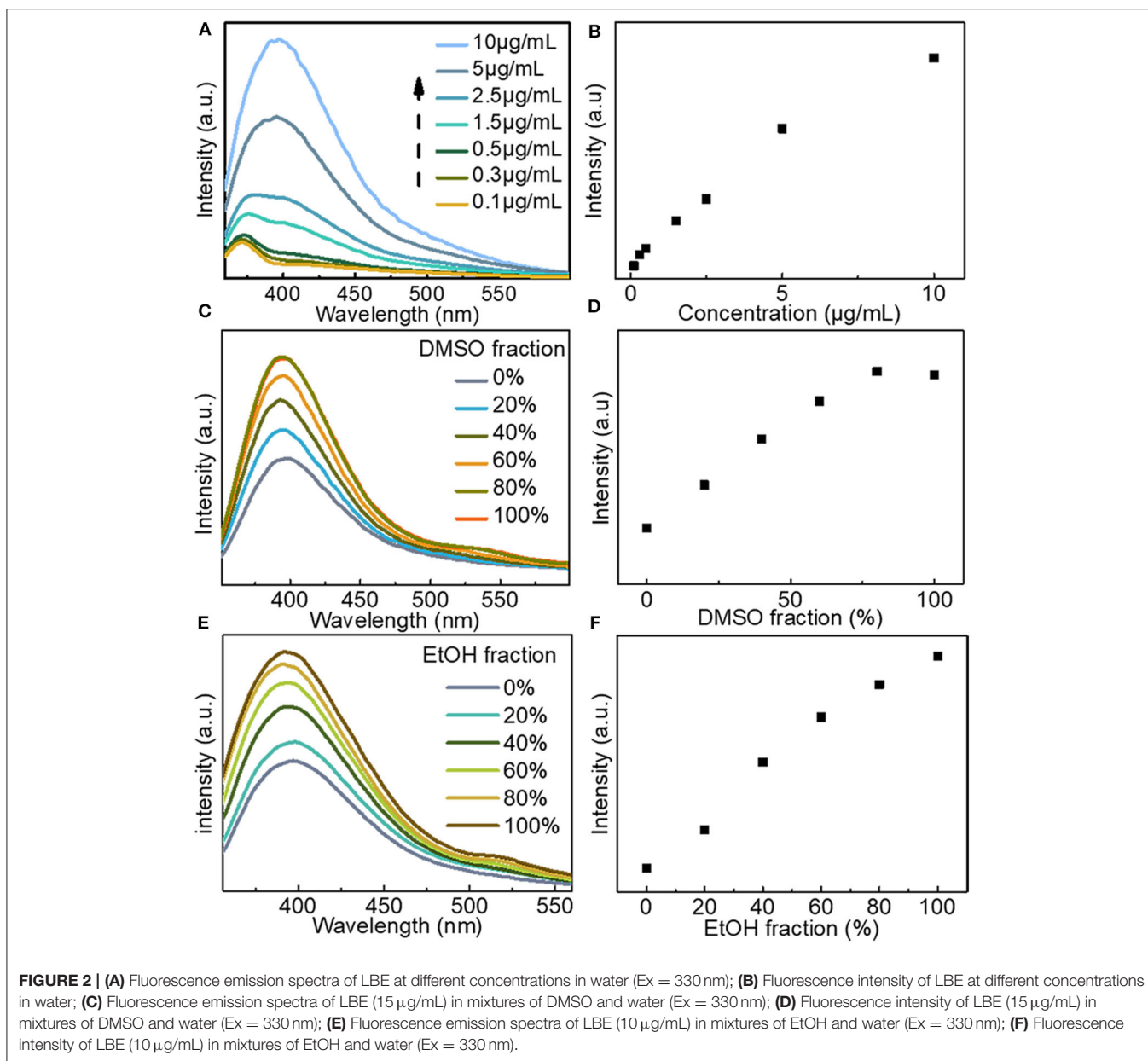
3.05–7.44 (Figure S8) of the intracellular microenvironments (Cosnier et al., 2013), suggesting that LBE was suitable for cellular imaging.

The toxicity of different concentrations of LBE toward MG-63 cells was investigated. LBE possessed growth effect on cells due to the good biological activity (Jiang et al., 2014, 2016). Incubation with LBE (1 mg/mL) for 24 h exhibited little effect on the survival of MG-63 cells, indicating that LBE was not toxic to MG-63 cells (Figure 5). Flow cytometry for 3 day showed that the total apoptosis of MG-63 cells in the early and late stages was 9.2% (Q2+Q4; Figure S9), confirming that LBE was non-toxic.

Confocal laser scanning microscopy (CLSM) was utilized to monitor uptake of LBE by MG-63 cells over 10 h at 37°C (Figure 6). Figure 6A shows cell nuclei stained with DAPI and

Figure 6B shows cells incubated with LBE nanoparticles, respectively. Figure 6C, which shows these two images superimposed, demonstrates that LBE nanoparticles efficiently crossed the cell membrane and became localized in the cell nucleus. Therefore, LBE nanoparticles can be employed as a fluorescent dye to stain nucleus.

The effect of different metal ions on the fluorescence intensity of an aqueous solution of LBE was investigated to explore the possible application of LBE in the detection of metal ions. Fe^{3+} ions were found to quench the fluorescence markedly, while the interference effect of other ions on fluorescence showed a slight or no effect (Figure 7A and Figure S10), which revealed that the LBE possessed a satisfying selectivity for the assay of Fe^{3+} . Since the phenolic hydroxyl groups in LBE molecule could form complexes with Fe^{3+} ions as an electron donor, which was



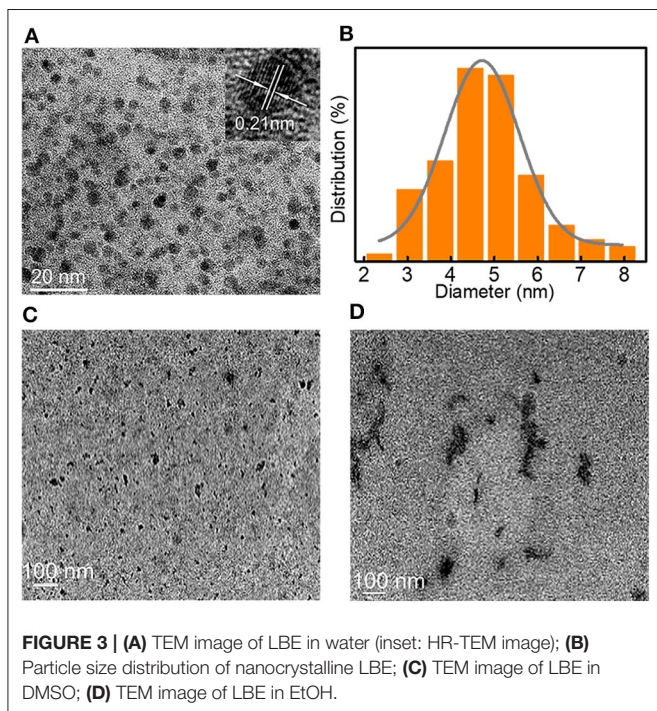
beneficial to facilitate charge transfer (Guo et al., 2015; Shen et al., 2017). The recombination of excitons was inhibited and then a significant fluorescence quenching occurred (Zhang Y. L. et al., 2013; Wang et al., 2018). **Figure 7B** and **Figure S10** showed the relative fluorescence response of LBE (I_0/I) according to the concentration of Fe^{3+} , where I_0 and I are the fluorescence intensities of LBE in the absence and presence of Fe^{3+} ions, respectively. The fluorescence quenching efficiency is described by Stern-Volmer plot (Sachdev and Gopinath, 2015; Arumugham et al., 2020). A good linear relationship with the correlation coefficient squared (R^2) of 0.9894 was observed when the concentration of Fe^{3+} changed from 0 to 128 µM (**Figure 7B**). The limitation of detection (LOD) was estimated to be 0.17 µM based on the signal-to-noise ratio (SNR) of 3 ($3\sigma/m$, σ is the

standard deviation of the blank signal ($n = 3$) and m is the slope of the linear fit). This value is well below the maximum allowable level of Fe^{3+} in drinking water set by the World Health Organization (5.36 µM). Moreover, the method of detecting Fe^{3+} based on carbon dots in this article was comparable or even better than that in other previous reports (Shen et al., 2017; Chen et al., 2019; Arumugham et al., 2020). The results indicated that LBE owned a good application prospect in the detection of trace Fe^{3+} due to the low LOD of Fe^{3+} (Wang et al., 2018).

CONCLUSIONS

Larch bark is a natural biomass resource typically regarded as waste. Here, we used a simple method to convert larch

bark into LBE nanoparticles, which showed aggregation-induced luminescence in solution. Enhancement of fluorescence emission was observed at high concentrations, in poor solvents, at low temperatures and in highly viscous solvents. Solutions of LBE were resistant to photobleaching under strong UV irradiation. Notably, LBE possessed good biocompatibility and exhibited no obvious toxicity to MG-63 cells, even at a high concentration (1 mg/mL). LBE could be used as a biological chromogenic fluorescent staining agent for cell nuclei. Additionally, Fe^{3+} ions were found to own a marked quenching effect on the fluorescence of LBE solutions. The limitation of detection (LOD) was $0.17 \mu\text{M}$ so that LBE possessed a good application prospect in the detection of trace Fe^{3+} .



METHODS

Preparation of LBE

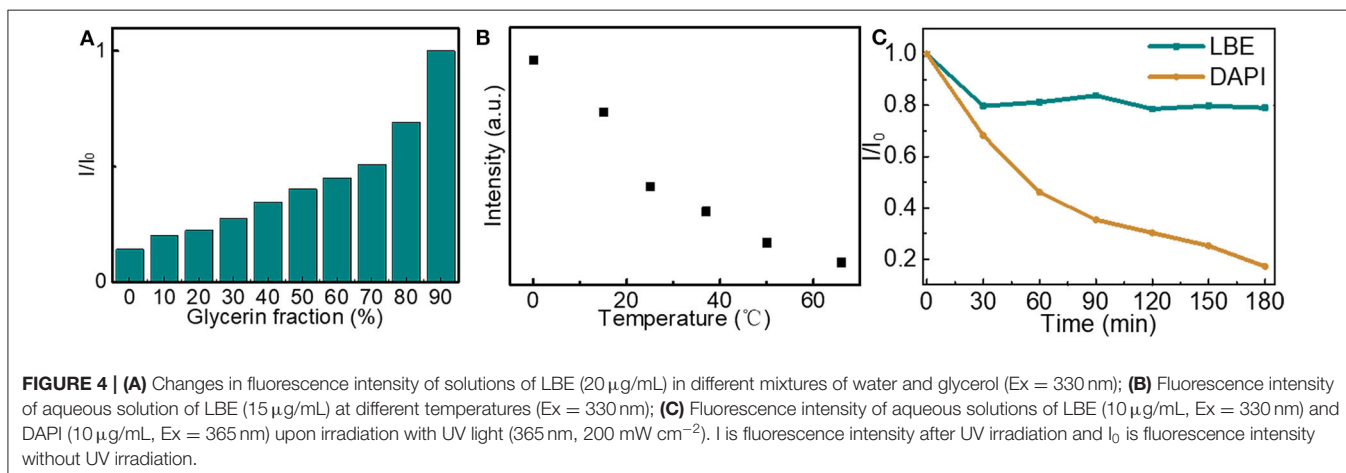
Larch bark powder (3 g) was extracted with 40% aqueous ethanol (60 mL) for 25 min at $50\text{--}55^\circ\text{C}$ using scientz-1,200e ultrasonic cell grinder, operating at 500 W. The extract was separated by centrifugation and the larch bark was re-extracted as described above. The combine two extraction solutions that the combined extracts were dialyzed with deionized water (1 L) for 3 days under magnetic stirring using a dialysis bag (MWCO: 3500 Da). The external dialysate was concentrated and freeze-dried to give LBE as a brown solid.

Characterization

The extraction is carried out by scientz-1,200e ultrasonic cell grinder. TEM and HR-TEM images were collected using a JEM-2,100 transmission electron microscope. X-ray photoelectron spectroscopy (XPS) was carried out using an Escalab 250Xi X-ray photoelectron spectrometer. FTIR spectra were recorded using a Frontier Fourier transform infrared spectrometer. UV-vis absorption spectra were recorded using a TU-1950 ultraviolet-visible spectrofluorometer. Photoluminescence (PL) measurements were carried out using an LS55 fluorescence spectrometer. Fluorescence decay curves were measured using a DeltaFlex modular fluorescence lifetime instrument. PL quantum yields were measured using an FLS1000 fluorescence spectrometer. Fluorescence images were captured using a DMI4000 B inverted fluorescence microscope. The molecular weight distribution of LBE was measured using an AutoflexIII mass spectrometer.

Cytotoxicity Test

The effects of different concentrations of LBE on the viability of MG-63 cells were determined using a Cell Counting Kit-8 (CCK-8) assay. Cell suspensions, harvested at the exponential growth phase of the cells, were plated onto a 96-well plate at a density of 5,000 cells per well. The cells were then grown overnight at 37°C in culture medium (10% FBS + 90% DMEM/F12 + $100 \mu\text{g/mL}$ Normocin) in a humidified atmosphere of 5% CO_2 to ensure that the cells adhered to the orifice plates. The wells were then divided



into a blank control group (medium only), a negative control group (medium + cells) and 8 test groups (medium + cells + LBE), with 8 wells in each group. In the test groups, the cells were cultured in the presence of different concentrations (0, 12.5, 25, 50, 100, 200, 400, 800, 1,000 $\mu\text{g}/\text{mL}$) of LBE. The cells were placed in an incubator at 37°C in a humidified atmosphere of 5% CO_2

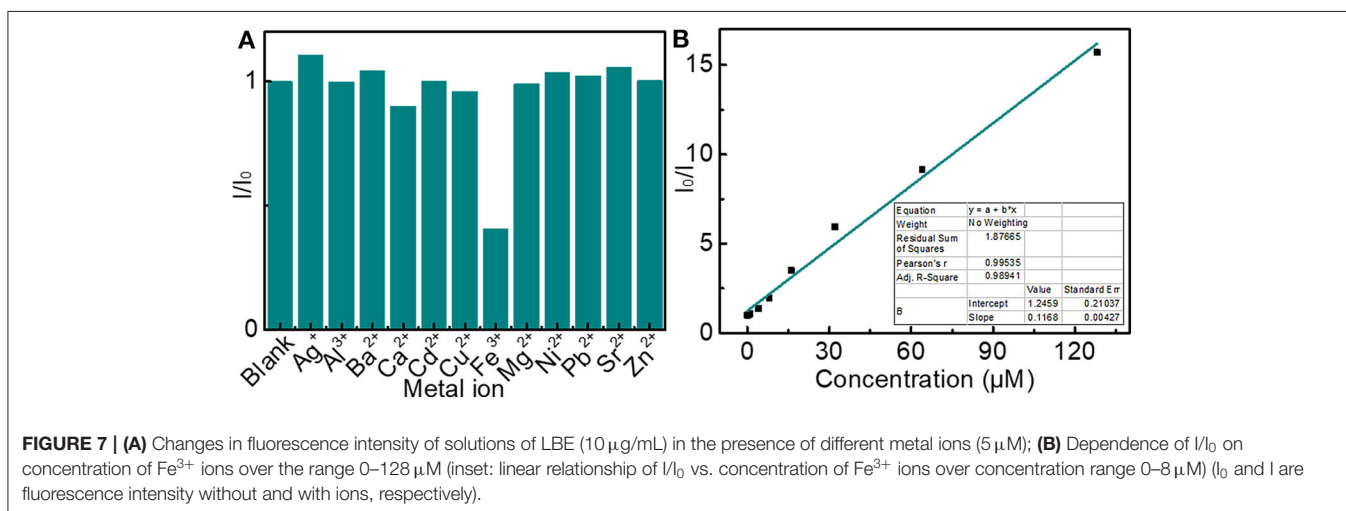
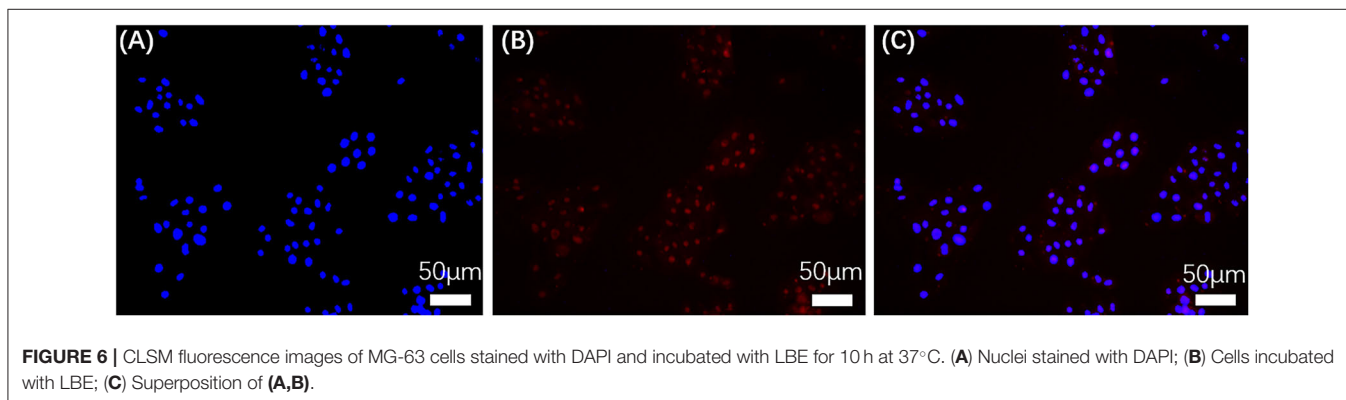
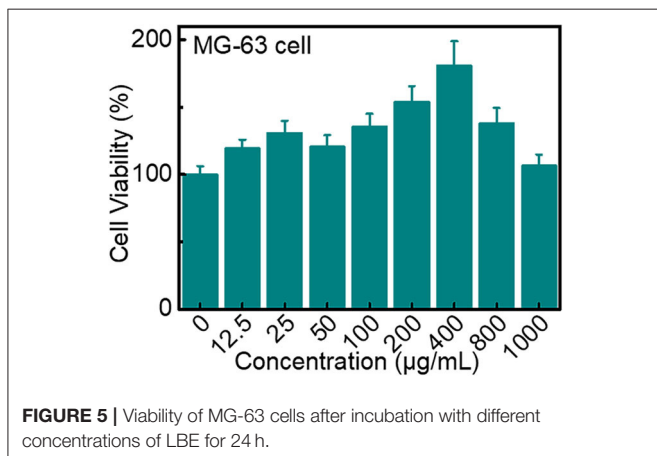
for 24 h. CCK-8 (10 μL) was then added to each well and the cells were incubated for a further 4 h at 37°C . The absorbance of each well was measured at 450 nm using a Multiskan GO microplate reader (Thermo Fisher Scientific, Vantaa, Finland). Cell viability was defined as the ratio of absorbance in the presence of LBE to that in the absence LBE.

Cell viability (%)

$$= \frac{OD_{test} - OD_{blank\ control}}{OD_{negative\ control} - OD_{blank\ control}} \times 100\% \quad (1)$$

Cellular Imaging

MG-63 cells were inoculated into 48-well plates (10,000 cells per well) with clean cover glasses. The cells were then grown for 24 h at 37°C in culture medium (10% FBS + 90% DMEM/F12 + 100 $\mu\text{g}/\text{mL}$ Normocin) in a humidified atmosphere of 5% CO_2 . LBE was added and the cells were cultured in a saturated humidity incubator at 37°C under an atmosphere of 5% CO_2 for 10 h. The cover glasses were removed and washed three times with PBS. The cells were immobilized with pre-cooled 4% paraformaldehyde solution for 30 min and then dyed using a solution of DAPI in PBS (10 $\mu\text{g}/\text{mL}$) for 5 min. After each operation, the cover glasses were washed three times with PBS. The cover glasses were sealed with anti-fluorescence



quenching agent and images were captured using an inverted fluorescence microscope.

Sensing of Fe³⁺ and Other Ions

Three mL of LBE solution with concentration 10 μg/mL was put into a four-way quartz cuvette with a lid, then added 20 μL of Fe³⁺ solution with different concentrations by means of a pipette to make the Fe³⁺ concentration range from 0 to 128 μL. All the obtained solutions were shaken evenly, and then the fluorescence emission spectrum (Ex = 330nm) was measured after standing for 1 min. Similarly, other metal ions were also analyzed in this way and they were newly prepared like the Fe³⁺ solution of different concentrations.

Materials and Reagents

Larch bark was obtained from deciduous pines of the Daxing'an Mountains, Heilongjiang Province, China. All reagents were analytical reagent grade and were used as received without further purification. Deionized water was prepared using a Clever-Q30 UT water filtration system (Zhiang Instrument Co., Ltd. Shanghai, China). A Cell Counting Kit-8 (CCK-8) assay kit was purchased from Dojindo Laboratories (Kumamoto, Japan) and Normocin was purchased from InvivoGen (San Diego, CA, USA). Fetal bovine serum (FBS), Dulbecco's modified Eagle's medium/Ham's F-12 medium (DMEM/F12) and phosphate buffered saline (PBS) were Gibco reagents and were purchased from Thermo Fisher Scientific Inc. (Waltham, MA, USA). MG-63 cells was purchased from the Chinese Academy of Sciences (Shanghai, China).

REFERENCES

- An, L. L., Si, C. L., Wang, G. H., Sui, W. J., and Tao, Z. Y. (2019). Enhancing the solubility and antioxidant activity of high-molecular-weight lignin by moderate dpolymerization via *in situ* ethanol/acid catalysis. *Indus. Crops Products* 128, 177–185. doi: 10.1016/j.indcrop.2018.11.009
- Arumugham, T., Alagumuthu, M., Amimodu, R. G., Munusamy, S., and Iyer, S. K. (2020). A sustainable synthesis of green carbon quantum dot (CQD) from catharanthus roseus (white flowering plant) leaves and investigation of its dual fluorescence responsive behavior in multi-ion detection and biological applications. *SMT* 23:e00138. doi: 10.1016/j.susmat.2019.e00138
- Bao, L., Liu, C., Zhang, Z. L., and Pang, D. W. (2015). Photoluminescence-tunable carbon nanodots: surface-state energy-gap tuning. *Adv. Mater.* 27, 1663–1667. doi: 10.1002/adma.201405070
- Bi, Z. H., Li, T. W., Su, H., Ni, Y., and Yan, L. F. (2018). Transparent wood film incorporating carbon dots as encapsulating material for white light-emitting diodes. *ACS Sustainable Chem. Eng.* 6, 9314–9323. doi: 10.1021/acssuschemeng.8b01618
- Chang, Q., Ding, Y., Cheng, S., Shen, W., Zhou, Z., Yin, Y. H., et al. (2019). Quench-resistant and stable nanocarbon dot/sheet emitters with tunable solid-state fluorescence via aggregation-induced color switching. *Nanoscale* 11, 2131–2137. doi: 10.1039/C8NR08429G
- Chen, J., Wei, J. S., Zhang, P., Niu, X. Q., Zhao, W., Zhu, Z. Y., et al. (2017). Red-emissive carbon dots for fingerprints detection by spray method: coffee ring effect and unquenched fluorescence in drying process. *ACS Appl. Mater. Interfaces* 9, 18429–18433. doi: 10.1021/acsmi.7b03917
- Chen, Y. H., Zheng, M. T., Xiao, Y., Dong, H. W., Zhang, H. R., Zhuang, J. L., et al. (2016). A self-quenching-resistant carbon-dot powder with tunable solid-state

DATA AVAILABILITY STATEMENT

All datasets generated for this study are included in the article/**Supplementary Material**.

AUTHOR CONTRIBUTIONS

JN and YH conducted the extract experiments. ZP performed the cell imaging experiments. SH, MG, and GJ carried out characterization and analysis of the samples. SH and CZ wrote the manuscript and made substantial revisions. Supervision, funding acquisition, review, and editing of the manuscript were carried out by SL and JC. All authors have approved the final version of the manuscript.

FUNDING

This work was supported by the National Natural Science Foundation of China (31870553), the Key Research and Development Planning Projects of Jilin Province in the Agricultural Field (20190301045N Y), and the Industrial Innovation Special Fund Project of Development and Reform Commission in Jilin Province (2019C044-4). The authors are grateful for the funding.

SUPPLEMENTARY MATERIAL

The Supplementary Material for this article can be found online at: <https://www.frontiersin.org/articles/10.3389/fchem.2020.00563/full#supplementary-material>

- fluorescence and construction of dual-fluorescence morphologies for white light-emission. *Adv. Mater.* 28, 312–318. doi: 10.1002/adma.201503380
- Chen, Y. Q., Sun, X. B., Pan, W., Yu, G. F., and Wang, J. P. (2019). Fe³⁺-sensitive carbon dots for detection of Fe³⁺ in aqueous solution and intracellular imaging of Fe³⁺ inside fungal cells. *Front. Chem.* 7:911. doi: 10.3389/fchem.2019.00911
- Chiang, C. L., Wu, M. F., Dai, D. C., Wen, Y. S., Wang, J. K., and Chen, C. T. (2005). Red-emitting fluorenes as efficient emitting hosts for non-doped, organic red-light-emitting diodes. *Adv. Funct. Mater.* 15, 231–238. doi: 10.1002/adfm.200400102
- Cosnier, S., Goff, A. L., and Holzinger, M. (2013). Towards glucose biofuel cells implanted in human body for powering artificial organs: review. *Electrochem. Commun.* 38, 19–23. doi: 10.1016/j.elecom.2013.09.021
- Ding, H., Wei, J. S., Zhang, P., Zhou, Z. Y., Gao, Q. Y., and Xiong, H. M. (2018). Solvent-controlled synthesis of highly luminescent carbon dots with a wide color gamut and narrowed emission peak widths. *Small* 14:1800612. doi: 10.1002/sml.201800612
- Ding, H., Yu, S. B., Wei, J. S., and Xiong, H. M. (2016). Full-color light-emitting carbon dots with a surface-state-controlled luminescence mechanism. *ACS Nano* 10, 484–491. doi: 10.1021/acsnano.5b05406
- Du, H. H., Liu, W., Zhang, M. M., Si, C. L., Zhang, X. Y., and Li, B. (2019). Cellulose nanocrystals and cellulose nanofibrils based hydrogels for biomedical applications. *Carbohydr. Polym.* 209, 130–144. doi: 10.1016/j.carbpol.2019.01.020
- Gu, K. Z., Xu, Y. S., Li, H., Guo, Z. Q., Zhu, S. J., Zhu, S. Q., et al. (2016). Real-time tracking and *in vivo* visualization of β-galactosidase activity in colorectal tumor with a ratiometric near-infrared fluorescent probe. *J. Am. Chem. Soc.* 138, 5334–5340. doi: 10.1021/jacs.6b01705

- Gujt, J., Vargas, E. C., Puszta, L., and Pizio, O. (2017). On the composition dependence of thermodynamic, dynamic and dielectric properties of water-dimethyl sulfoxide model mixtures. NPT molecular dynamics simulation results. *J. Mol. Liq.* 228, 71–80. doi: 10.1016/j.molliq.2016.09.024
- Guo, Y. M., Zhang, L. F., Yang, Y., Chen, X. H., and Zhang, M. C. (2015). Fluorescent carbon nanoparticles for the fluorescent detection of meta lions. *Biosens Bioelectron.* 63, 61–71. doi: 10.1016/j.bios.2014.07.018
- He, T., Niu, N., Chen, Z. J., Li, S. J., Liu, S. X., and Li, J. (2018). Novel quercetin aggregation-induced emission luminogen (AIEgen) with excited-state intramolecular proton transfer for *in vivo* bioimaging. *Adv. Funct. Mater.* 28:1706196. doi: 10.1002/adfm.201706196
- Hong, Y., Lam, J. W. Y., and Tang, B. Z. (2009). Aggregation-induced emission: phenomenon, mechanism and applications. *Chem. Commun.* 4332–4353. doi: 10.1039/b904665h
- Hu, R. R., Leung, N. L. C., and Tang, B. Z. (2014). AIE macromolecules: syntheses, structures and functionalities. *Chem. Soc. Rev.* 43, 4494–4562. doi: 10.1039/C4CS00044G
- Jara, P. J., and Josep, L. T. (2012). Analysis of proanthocyanidins in almond blanch water by HPLC–ESI–QqQ–MS/MS and MALDI–TOF/TOF MS. *Food Res. Intern.* 49, 798–806. doi: 10.1016/j.foodres.2012.09.005
- Jiang, G. Q., Fang, G. Z., Li, L. L., Shi, Z. X., and Zhang, Z. R. (2014). Study on antioxidant activity of catalyzed hydrogen degradation product of polymeric proanthocyanidins (LPPC) from larix gmelinii bark. *BioResources* 9, 662–672. doi: 10.15376/biores.9.1.662-672
- Jiang, G. Q., Zhang, Z. R., Li, L. L., Du, F. G., and Pang, J. Y. (2016). Analysis of purified oligomeric proanthocyanidins from larix gmelinii bark and the study of physiological activity of the purified product. *BioResources* 11, 1690–1706. doi: 10.15376/biores.11.1.1690-1706
- Krueger, C. G., Vestling, M. M., and Reed, J. D. (2003). Matrix-assisted laser desorption/ionization time-of-flight mass spectrometry of heteropolyflavan-3-ols and glucosylated heteropolyflavans in Sorghum [Sorghum bicolor (L.) moench]. *J. Agric. Food Chem.* 51, 538–543. doi: 10.1021/jf020746b
- Lee, Y. T., Chang, Y. T., Chen, C. T., and Chen, C. T. (2016). The first aggregation-induced emission fluorophore as a solution processed host material in hybrid white organic light-emitting diodes. *J. Mater. Chem. C* 4, 7020–7025. doi: 10.1039/C6TC01251E
- Li, M., An, X. F., Jiang, M. Y., Li, S. J., Liu, S. X., Chen, Z. J., et al. (2019a). “Cellulose spacer” strategy: anti-aggregation-caused quenching membrane for mercury detection and removal. *ACS Sustainable Chem. Eng.* 7, 15182–15189. doi: 10.1021/acssuschemeng.9b01928
- Li, M., Li, X. N., An, X. F., Chen, Z. J., and Xiao, H. N. (2019b). Clustering-triggered emission of carboxymethylated nanocellulose. *Front. Chem.* 7, 447. doi: 10.3389/fchem.2019.00447
- Li, X. Y., Xua, R., Yang, J. X., Nie, S. X., Liu, D., Liu, Y., et al. (2019c). Production of 5-hydroxymethylfurfural and levulinic acid from lignocellulosic biomass and catalytic upgradation. *Indus. Crops Products* 130, 184–197. doi: 10.1016/j.indcrop.2018.12.082
- Liu, B., Duan, H. Y., Wang, Y. L., Du, B. Y., Yang, Q., Xu, J. T., et al. (2018). A fluorescein-centered polymer as a phosphor for fabricating pure white light-emitting diodes. *Mater. Horiz.* 5, 932–938. doi: 10.1039/C8MH00749G
- Lou, X. D., Zhao, Z. J., and Tang, B. Z. (2016). Organic dots based on AIEgens for two-photon fluorescence bioimaging. *Small* 12, 6430–6450. doi: 10.1002/sml.201600872
- Lu, H. G., Su, F. Y., Mei, Q., Tian, Y. Q., Tian, W. J., Johnson, R. H., et al. (2012). Using fluorine-containing amphiphilic random copolymers to manipulate the quantum yields of aggregation-induced emission fluorophores in aqueous solutions and the use of these polymers for fluorescent bioimaging. *J. Mater. Chem.* 22, 9890–9900. doi: 10.1039/c2jm30258f
- Luo, X. F., Ma, C. H., Chen, Z. J., Zhang, X. Y., Niu, N., Li, J., et al. (2019). Biomass-derived solar-to-thermal materials: promising energy absorbers to convert light to mechanical motion. *J. Mater. Chem. A* 7, 4002–4008. doi: 10.1039/C8TA11199E
- María, M., Jesús, E. Q. L., Garmen, G. G., Begona, B., and Rosa, L. A. (2010). MALDI-TOF MS analysis of plant proanthocyanidins. *J. Pharm. Biomed. Anal.* 51, 358–372. doi: 10.1016/j.jpba.2009.03.035
- Mei, J., Hong, Y. N., Lam, J. W. Y., Qin, A. J., Tang, Y. H., and Tang, B. Z. (2014). Aggregation-induced emission: the whole is more brilliant than the parts. *Adv. Mater.* 26, 5429–5479. doi: 10.1002/adma.201401356
- Miao, X., Qu, D., Yang, D. X., Nie, B., Zhao, Y. K., Fan, H. Y., et al. (2018). Synthesis of carbon dots with multiple color emission by controlled graphitization and surface functionalization. *Adv. Mater.* 30:1704740. doi: 10.1002/adma.201704740
- Ouchemoukh, S., Hachoud, S., Boudraham, H., Mokrani, A., and Louaiche, H. (2012). Antioxidant activities of some dried fruits consumed in Algeria. *Food Res. Intern.* 49, 329–332. doi: 10.1016/j.lwt.2012.07.022
- Park, S. J., Yang, H. K., and Moon, B. K. (2019). Ultraviolet to blue blocking and wavelength convertible films using carbon dots for interrupting eye damage caused by general lighting. *Nano Energy* 60, 87–94. doi: 10.1016/j.nanoen.2019.03.043
- Qi, H. J., Teng, M., Liu, M., Liu, S. X., Li, J., Yu, H. P., et al. (2019). Biomass-derived nitrogen-doped carbon quantum dots: highly selective fluorescent probe for detecting Fe³⁺ ions and tetracyclines. *J. Colloid Interface Sci.* 539, 332–341. doi: 10.1016/j.jcis.2018.12.047
- Qu, S. N., Chen, H., Zheng, X. M., Cao, J. S., and Liu, X. Y. (2013). Ratiometric fluorescent nanosensor based on water soluble carbon nanodots with multiple sensing capacities. *Nanoscale* 5, 5514–5518. doi: 10.1039/c3nr00619k
- Sachdev, A., and Gopinath, P. (2015). Green synthesis of multifunctional carbon dots from coriander leaves and their potential application as antioxidants, sensors and bioimaging agents. *Analyst* 140, 4260–4269. doi: 10.1039/C5AN00454C
- Sharma, S. D., Meeran, S. M., and Katiyar, S. K. (2010). Proanthocyanidins inhibit *in vitro* and *in vivo* growth of human non-small cell lung cancer cells by inhibiting the prostaglandin E (2) and prostaglandin E (2) receptors. *Mol. Cancer Ther.* 9, 569–580. doi: 10.1158/1535-7163.MCT-09-0638
- Shen, J., Shang, S. M., Chen, X. Y., Wang, D., and Cai, Y. (2017). Facile synthesis of fluorescence carbon dots from sweet potato for Fe³⁺ sensing and cell imaging. *Mat. Sci. Eng. C Mater.* 76, 856–864. doi: 10.1016/j.msec.2017.03.178
- Sheng, Z. H., Shao, L., Chen, J. J., Bao, W. J., Wang, F. B., and Xia, X. H. (2011). Catalyst-free synthesis of nitrogen-doped graphene via thermal annealing graphite oxide with melamine and its excellent electrocatalysis. *ACS Nano.* 5, 4350–4358. doi: 10.1021/nn103584t
- Shoji, T., Masumoto, S., Moriichi, N., Kanda, T., and Ohtake, Y. (2006). Apple (Malus pumila) procyanidins fractionated according to the degree of polymerization using normal-phase chromatography and characterized by HPLC–ESI/MS and MALDI–TOF/MS. *J. Chromatogr. A* 1102, 206–213. doi: 10.1016/j.chroma.2005.10.065
- Tachibana, H., Aizawa, N., Hidaka, Y., and Yasuda, T. (2017). Tunable full-color electroluminescence from all-organic optical upconversion devices by near-infrared sensing. *ACS Photonics* 4, 223–227. doi: 10.1021/acsp Photonics.6b00964
- Wang, W. L., Wang, Z., f., Liu, J. J., Peng, Y. K., Yu, X. Y., et al. (2018). One-pot facile synthesis of graphene quantum dots from rice husks for Fe³⁺ sensing. *Ind. Eng. Chem. Res.* 57, 9144–9150. doi: 10.1021/acs.iecr.8b00913
- Wang, Y., Kalytchuk, S., Zhang, Y., Shi, H. C., Kershaw, S. V., and Rogach, A. L. (2014). Thickness-dependent full-color emission tunability in a flexible carbon dot ionogel. *J. Phys. Chem. Lett.* 5, 1412–1420. doi: 10.1021/jz5005335
- Wang, Z. K., Chen, S. J., Lam, J. W. Y., Qin, W., Kwok, R. T. K., Xie, N., et al. (2013). Long-term fluorescent cellular tracing by the aggregates of AIE bioconjugates. *J. Am. Chem. Soc.* 135, 8238–8245. doi: 10.1021/ja312581r
- Wu, Y. S., Zhang, H., Pan, A. Z., Wang, Q., Zhang, Y. F., and Zhou, G. J. (2019). White-light-emitting melamine-formaldehyde microspheres through polymer-mediated aggregation and encapsulation of graphene quantum dots. *Adv. Sci.* 6:1801432. doi: 10.1002/advs.201801432
- Yang, H. Y., Liu, Y. L., Guo, Z. Y., Lei, B. F., Zhuang, J. L., Zhang, X. J., et al. (2019). Hydrophobic carbon dots with blue dispersed emission and red aggregation-induced emission. *Nat. Commun.* 10:1789. doi: 10.1038/s41467-019-09830-6
- Yang, Y., and Chien, M. J. (2000). Characterization of grape procyanidins using high-performance liquid chromatography/mass spectrometry and matrix-assisted laser desorption/ionization time-of-flight mass spectrometry. *J. Agric. Food Chem.* 48, 3990–3996. doi: 10.1021/jf000316q
- Zhang, H., Zheng, X., Xie, N., He, Z., Liu, J., Leung, N. L. C., et al. (2017). Why do simple molecules with “isolated” phenyl rings emit visible light? *J. Am. Chem. Soc.* 139, 16264–16272. doi: 10.1021/jacs.7b08592
- Zhang, H. J., Chen, Y. L., Liang, M. J., Xu, L. F., Qi, S. D., Chen, H. L., et al. (2014). Solid-phase synthesis of highly fluorescent nitrogen-doped carbon dots for sensitive and selective probing ferric ions in living cells. *Anal. Chem.* 86, 9846–9852. doi: 10.1021/ac502446m

- Zhang, N., Li, W. Z., Chen, C., and Zuo, J. G. (2013). Molecular dynamics simulation of aggregation in dimethyl sulfoxide-water binary mixture. *Comput. Theoret. Chem.* 1017, 126–135. doi: 10.1016/j.comptc.2013.05.018
- Zhang, T. Y., Zhao, F. F., Li, L., Qi, B., Zhu, D. X., Lu, J. H., et al. (2018). Tricolor white-light-emitting carbon dots with multiple-cores@shell structure for WLED application. *ACS Appl. Mater. Interfaces* 10, 19796–19805. doi: 10.1021/acsami.8b03529
- Zhang, Y. L., Wang, L., Zhang, H. C., Liu, Y., Wang, H. Y., Kang, Z. H., et al. (2013). Graphitic carbon quantum dots as a fluorescent sensing platform for highly efficient detection of Fe³⁺ ions. *RSC Adv.* 3, 3733–3738. doi: 10.1039/c3ra23410j
- Zhu, S. J., Meng, Q. N., Wang, L., Zhang, J. H., Song, Y. B., Jin, H., et al. (2013). Highly photoluminescent carbon dots for multicolor patterning, sensors, and bioimaging. *Angew. Chem. Int. Ed.* 52, 3953–3957. doi: 10.1002/anie.201300519
- Zhu, S. J., Song, Y. B., Wang, J., Wan, H., Zhang, Y., Ning, Y., et al. (2016). Photoluminescence mechanism in graphene quantum dots: quantum confinement effect and surface/edge state. *Nano Today* 13, 10–14. doi: 10.1016/j.nantod.2016.12.006

Conflict of Interest: The authors declare that the research was conducted in the absence of any commercial or financial relationships that could be construed as a potential conflict of interest.

Copyright © 2020 Han, Ni, Han, Ge, Zhang, Jiang, Peng, Cao and Li. This is an open-access article distributed under the terms of the Creative Commons Attribution License (CC BY). The use, distribution or reproduction in other forums is permitted, provided the original author(s) and the copyright owner(s) are credited and that the original publication in this journal is cited, in accordance with accepted academic practice. No use, distribution or reproduction is permitted which does not comply with these terms.